

# Engineered Doxorubicin Delivery System Using Proteinoid-Poly (L-Lactic Acid) Polymeric Nanoparticles of Narrow Size Distribution and High Molecular Weight for Cancer Treatment

Stella Kiel<sup>1</sup>, Michal Kolitz-Domb<sup>1</sup>, Enav Corem-Salkmon, Igor Grinberg and Shlomo Margel\*

<sup>1</sup>These authors contributed equally to this study

The Institute of Nanotechnology and Advanced Materials, Department of Chemistry, Bar-Ilan University, Ramat-Gan, 52900, Israel

## \*Corresponding author

Shlomo Margel, The Institute of Nanotechnology and Advanced Materials, Department of Chemistry, Bar-Ilan University, Ramat-Gan, 52900, Israel, Tel: + 972-3-5318861, E-mail: shlomo.margel@mail.biu.ac.il

Submitted: 27 Apr 2017; Accepted: 03 May 2017; Published: 07 May 2017

## Abstract

Doxorubicin (Dox), a widely used anti-cancer drug, was encapsulated within new special-tailored proteinoid nanoparticles (NPs), with the intention to overcome side effects while keeping the drug potency. The synthesis and characterization of four newly-made proteinoids of very high molecular weights (122-149 kDa) and low polydispersity (1.01-1.03) is presented. The proteinoids were synthesized from L-lysine, L-arginine, L-histidine, L-phenylalanine and poly-L-lactic acid (PLLA) segments, and are named P(KRHF-PLLA). Using this selection of amino acids provides basic positive-charged novel tailored proteinoids, with a rigid and biodegradable backbone, achieved by the incorporation of PLLA. The proteinoids self-assemble to yield NPs of a narrow-size distribution. This self-assembly procedure was utilized to encapsulate Dox within the NP core. The optimal Dox-encapsulated NPs were chosen by a study of their size, size distribution and Dox content. The chosen NPs, 15% Dox-loaded P(KRHF-PLLA) NPs were checked for their stability in different conditions. In order to improve tumor uptake and time of circulation in the blood, the chosen NPs were further PEGylated and the effects of PEGylation of the NPs, as well as the effect of the environment, on the release rate of Dox from the NPs were investigated. Additionally, the cytotoxicity of the PEGylated and non-PEGylated Dox-containing NPs was studied by XTT assay and their generation of immune-response was investigated by cytokines induction assay. Overall, the Dox-loaded NPs were found stable, non-immunogenic and showed good cell toxicity, making them good candidates to be used against cancer, while PEGylation improved all parameters.

**Keywords:** Proteinoid nanoparticles; self-assembly; doxorubicin; drug delivery; cancer treatment.

## List of abbreviations

a.u.	Arbitrary units
Arg	Arginine
cm	Centimeter
Da, kDa	Dalton, kilodalton
Dox	Doxorubicin
DLS	Dynamic light scattering
DSC	Differential scanning calorimetry
ELISA	Enzyme linked immunosorbent assay
EPR	Enhanced permeability and retention
FTIR, IR	Fourier transform infrared
g	gram
GPC	Gel permeation chromatography

h	Hour
His	Histidine
HPLC	High performance liquid chromatography
HSA	Human serum albumin
J	Joule
LPS, L6529	Lipopolysaccharides
Lys	Lysine
M	Molar
mg	Milligram
min	Minute
mL	Milliliter
Mn	Number average molecular mass
Mp	Molecular mass at the peak
Mw	Weight average molecular mass
MWCO	Molecular weight cut-off
N	Normal

N.D.	Not detectable
NHS-PEG-maleimide	O-[N-(6-maleimidohexanoyl)aminoethyl]-O'-[3-(N-succinimidylloxy)-3-oxopropyl] polyethylene glycol
NIR	Near infra-red
nm	Nanometer
NP	Nanoparticle
PDI	Polydispersity index
PEG	Polyethylene glycol
pg	Picogram
Phe	Phenylalanine
P(KRHF-PLLA) x:y	Poly(lysine-arginine-histidine-phenylalanine-PLLA), x:y represent the percent ratio arginine:histidine
PLLA	Poly-L-lactic acid
PBS	Phosphate buffered saline
PBMCs	Peripheral blood mononuclear cells
SEM	Scanning electron microscopy
Tdec	Temperature of decomposition
TGA	Thermogravimetric analysis
TLR4	Toll-like receptor 4
Tm	Melting temperature
UV	Ultraviolet
v/v	Volume/volume
XTT	2,3-bis-(2-methoxy-4-nitro-5-sulphophenyl)-2H-tetrazolium-5-carboxanilide
XRD	X-ray powder diffraction
μL	Microliter
μg	Microgram

## Introduction

Doxorubicin hydrochloride (Dox) is a cytotoxic anthracycline antibiotic which intercalates with the DNA and is commonly used in the treatment of a wide range of cancers, including different types of carcinomas, hematological malignancies, and soft-tissue sarcomas [1,2]. Although it is widely used, its use in chemotherapy has been limited, mainly due to severe side effects, including cardiotoxicity and nephrotoxicity [1-5]. Many research labs have been struggling with the need to avoid and overcome the Dox side effects, without reducing the drug potency, usually by developing nanosized biospecific drug carriers [1, 3, 6, 7]. The most important requirement for potential drug carriers is a combination of a high drug loading capacity and a long bloodstream circulation time [8]. Typically, using polyethylene glycol (PEG) grafting on the outer surfaces of the drug carriers prevents non-specific binding of serum proteins, and promotes escape from phagocytosis [9,10]. The nanometric size of these drug carriers allows their accumulation in tumors through the enhanced permeability and retention (EPR) effect [6]. One example of a nanosized drug carrier system of the Dox is Doxil, a liposomal formulation containing 12.5% Dox, which decreases its cardiotoxicity [11]. It was first to be approved in 1995 for the treatment of solid tumors [12,13]. Doxil consists of a PEG-lipid surface which guarantees prolonged circulation and improves the tumor uptake [14].

Proteinoids, polymers made of amino acids by thermal condensation polymerization, are unique synthetic polymers discovered by Fox and coworkers [15-17]. Natural or synthetic amino acids are polymerized by step-growth polymerization in a special procedure, which is initiated by heating the amino acids to melting. The polymerization takes place at a high temperature, 140-180 °C, in an inert atmosphere in absence of additives such as solvents or catalysts [16-21]. The accepted mechanism of this polymerization process is based on the role of lysine as a solvent for the other monomers, as it is condensed into the caprolactam under the high temperature conditions. The caprolactam initiates the polymerization with the rest of the present amino acids [15-17, 22]. A brief schematic description of the polymerization process is shown in Figure 1.

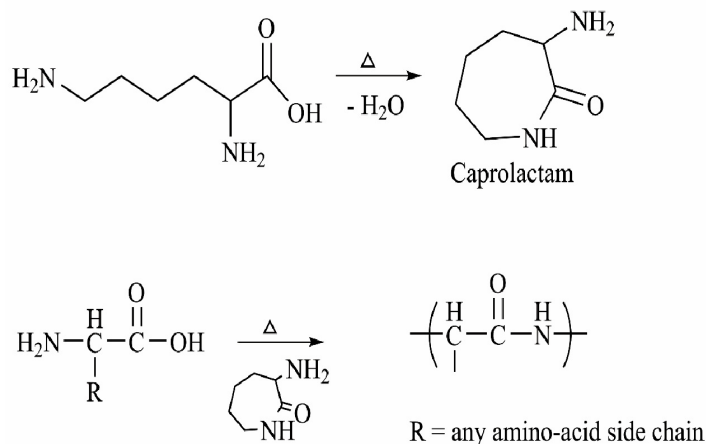


**Figure 1:** Preparation scheme of proteinoids by thermal polymerization of amino acids.

The proteinoids previously reported were of low molecular weights, up to approximately 10 kDa [16-19]. Post polymerization, the proteinoid may form micro- or nano-sized particles through a self-assembly procedure [23]. Briefly, the proteinoid is heated in aqueous conditions to dissolution and then slowly cooled to room temperature, leading to self-assembly into hollow nanoparticles [23]. If a suitable molecule is present during the particle formation, encapsulation of this molecule within the particle will occur [24], as presented in Figure 2.

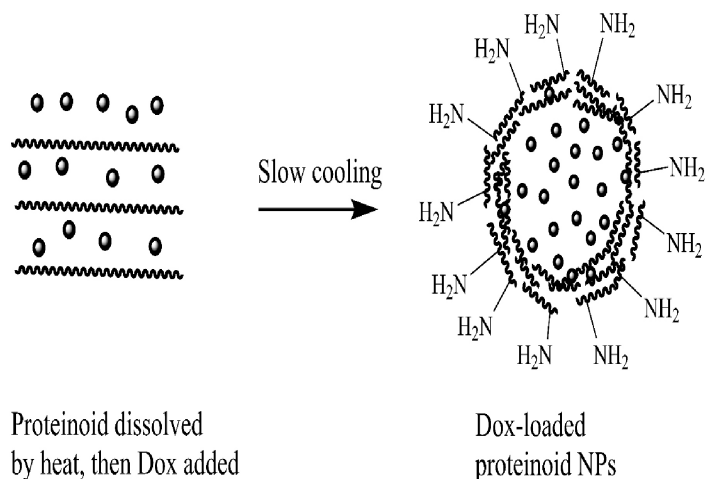


**Figure 2:** Schematic representation of the self-assembly of proteinoid particles; “hydrophobic moieties are represented by

scribbled lines, Dox is represented by the interior dots.

Recently, several kinds of proteinoids were investigated for use in the field of drug delivery [25, 26]. The proteinoid particles are biodegradable, considered to be non-immunogenic and they possess many chemically active groups on their surface. This enables conjugation to bioactive molecules which can specifically deliver the drug to its destination [27].

Previous studies of our group presented glutamic acid-based proteinoids of high molecular weights and very low polydispersity, which were stable, non-toxic and encapsulated the near-infrared fluorescent dye indocyanine green [23]. This way, NIR fluorescent proteinoid NPs were obtained and further utilized to tag tumor cells by conjugation to specific biomarkers [24, 28].

In the present study, several types of new proteinoids of high molecular weights and low polydispersity were synthesized from the natural amino acids lysine, arginine, histidine and phenylalanine in order to obtain new lysine-based proteinoids. PLLA was incorporated within the proteinoids to achieve enhanced biodegradability. The lysine-based proteinoids were used to encapsulate Dox to create anti-cancer nanoparticles (NPs) that can specifically detect and treat cancerous tumors. The Dox-loaded proteinoid NPs were studied in terms of size and size distribution, stability, cytotoxicity, drug release over time and immunogenicity.

## Materials and Methods

The following analytical-grade chemicals were purchased from commercial sources and used without further purification: L-lysine, L-arginine, L-histidine, L-phenylalanine, sodium chloride, sodium hydroxide 1N, hydrochloric acid 1N, Ficoll, lipopolysaccharides (LPS, L6529), Toll-like receptor 4 (TLR4), human serum albumin (HSA) and bovine plasma fibrinogen from Sigma (Rehovot, Israel); poly(L-lactic acid) (PLLA) MW 2 kDa from Polysciences (Warrington, PA, USA); phosphate buffered saline (PBS), PBS/- (calcium and magnesium free), glutamine, penicillin/streptomycin and mycoplasma detection kit from Biological Industries (Bet Haemek, Israel); cytotoxicity detection kit from Roche Diagnostics (Basel, Switzerland); dialysis membranes (1 kDa and 10 kDa MWCO), bicarbonate buffer (0.1 M, pH 8.4) and sodium bicarbonate from Bio-Lab Ltd. (Jerusalem, Israel); O-[N-(6-maleimidohexanoyl)aminoethyl]-O'-[3-(N-succinimidyl)-3-oxopropyl]polyethylene glycol (NHS-PEG-maleimide, MW 3 kDa) from JenKem Technology (Plano, TX, USA); CetriPUR pH 2 buffer solution (citric acid/ sodium hydroxide/ hydrogen chloride) from MERCK (Damstadt, Germany); human cell lines A172, HCT116 and MDA-MB-231 from the American Type Culture Collection (Manassus, VA, USA); human blood and Peripheral Blood Mononuclear Cells (PBMCs) obtained from Tel Hashomer (Sheba) blood bank (Ramat Gan, Israel); human IL-6, IL-10 and TNF- $\alpha$  ELISA kits from Ray Biotech (Norcross, GA, USA). Water was purified by passing deionized water through an Elgastat Spectrum reverse osmosis system from Elga Ltd. (High Wycombe, UK).

## Proteinoid Preparation by Thermal Condensation Polymerization

The proteinoid synthesis was generally similar to that described in our previous publication [23]. Briefly, L-lysine was heated to the molten state (140 °C) in a heating mantle, under a nitrogen atmosphere. The molten mass was stirred at 140 °C and to this

different contents of L-amino acids and PLLA were added to give a total monomer mass of 5 g. The mixture was mechanically stirred at 150 rpm for 1 h. The obtained product was a highly viscous amber-brown paste, which hardened upon cooling to room temperature. Then, 30 mL of super-purified water were added to the crude proteinoid, and the mixture was stirred for 2 h at room temperature, followed by intensive dialysis through a cellulose membrane (1 kDa MWCO) against super-purified water. The content of the dialysis tube was then lyophilized to yield the dried proteinoid powder. The compositions of the different poly(lysine-arginine-histidine-phenylalanine-PLLA), or P(KRHF-PLLA), are presented in Table 1.

**Table 1:** Amino acid content of the different proteinoids.

Polymer <sup>a</sup>	Amino acid content (weight % of total monomer) <sup>b</sup>				
	L-Lys(K)	L-Arg(R)	L-His(H)	L-Phe(F)	PLLA(2 kDa)
P(KRHF-PLLA) 35:15	25	15	35	15	10
P(KRHF-PLLA) 30:20	25	15	30	20	10
P(KRHF-PLLA) 25:25	25	15	25	25	10
P(KRHF-PLLA) 20:30	25	15	20	30	10

<sup>a</sup>Polymers made of lysine (K), arginine (R), histidine (H), phenylalanine (F) and PLLA; <sup>b</sup>numbers represent the varied percentages of histidine and phenylalanine, respectively, as the percentages of lysine, arginine and PLLA remain constant, 25%, 15% and 10%, respectively.

## Preparation of Hollow and Dox-loaded Proteinoid Nanoparticles

Proteinoid particles were prepared via a self-assembly process as previously described by our research group [29]. Briefly, 50 mg of the dried proteinoid were added to 5 mL of 10<sup>-5</sup> N NaCl solution. The mixture was then kept at 80 °C for 30 min to complete the dissolution of the proteinoid. Particle formation was achieved by removal of the heating, as the mixture was left to cool to room temperature. The Dox-loaded proteinoid NPs were obtained by the addition of Dox to the hot solution, prior to particle formation by self-assembly. Varying amounts (0, 10, 15, 25 and 30 weight % relative to the proteinoid) of Dox were dissolved in 0.5 mL of 10<sup>-5</sup> N NaCl solution and added to the heated solution of proteinoid (50 mg in 4.5 mL) to give a total volume of 5 mL. The excess drug was removed by extensive dialysis against super-purified water (10 kDa MWCO).

## Proteinoid and NPs Analysis

The molecular weights and polydispersity indices of the dried crude proteinoids were determined using Gel Permeation Chromatography (GPC) consisting of a Waters Spectra Series P100 isocratic HPLC pump with an ERMA ERC-7510 refractive index detector and a Rheodyne (Cotati, CA, USA) injection valve with a 20  $\mu$ L loop (Waters, MA, USA). The samples were eluted with super-pure HPLC water through a linear BioSep SEC-s3000 column (Phenomenex, CA, USA) at a flow rate of 1 mL/min, 80 °C. The molecular weights were determined relative to PEG standards (Polymer Standards Service, Silver Spring, MD, USA) with a molecular weight range of 100-450000 Da, human serum albumin (HSA, 67 kDa) and bovine plasma fibrinogen (340 kDa), using Clarity chromatography software (DataApex, Prague, Czech Republic). The optical activities of the proteinoids were determined using a PE 343 polarimeter (Perkin Elmer, MA, USA). All measurements were done in water, at 589 nm at 25 °C. The thermal behavior of the proteinoids, hollow, and Dox-loaded NPs was de-

terminated by Differential Scanning Calorimetry (DSC) and Thermogravimetric Analysis (TGA) using a TGA/DSC 1 STARe system (Mettler Toledo, Switzerland). This analysis was performed with approximately 8 mg of dried sample atmosphere (200 mL/min) at a heating rate of 10 °C/min under nitrogen atmosphere. The samples were heated from 25 to 600 °C.

The chemical structures of proteinoid, Dox-loaded NPs and free Dox were investigated by Fourier transform infrared (FTIR) spectroscopy. FTIR measurements of the crude proteinoids and proteinoid NPs were done using ALPHA-FTIR QuickSnap™ (Bruker, Israel). The analysis was performed with KBr pellets that contained 1% of the detected material relative to KBr. One hundred scans were performed at 4 cm<sup>-1</sup> resolution.

All the samples were checked for the presence of the crystalline and non-crystalline nature by exploiting X-ray diffraction (XRD). The XRD patterns were recorded using an X-ray diffractometer, model D8 Advance (Bruker, Israel) with Cu Ka radiation. Samples of free Dox and Dox-loaded NPs were recorded at equivalent Dox concentration.

The absorbance spectra of free Dox and Dox-loaded NPs were recorded in a pH 2 buffer and physiological pH (7.4), at 400-600 nm. The total concentration of free Dox and Dox-loaded NPs was 1 mg/mL. Absorbance spectra were obtained using a Cary 100 UV-Visible spectrophotometer (Agilent Technologies Inc., CA, USA).

The Dox loading content was determined by the following method: Dox-loaded NPs were lyophilized and then disrupted by an addition of a pH 2 buffer and sonication. The samples were analyzed by their absorbance spectra at 487 nm. Quantification was performed using a calibration curve of Dox standard solutions of known concentrations (0-125 µg/mL) in a pH 2 buffer at 487 nm (R<sup>2</sup> = 0.999). Each experiment was carried out in triplicate, and the average values were compared.

NP formation yield and drug entrapment efficiency were calculated using Equations (1) and (2), respectively:

$$1) \text{ Nanoparticle yield (\%)} = \frac{\text{Weight of NPs}}{\text{weight of proteinoid} + \text{drug fed initially}} \times 100\%$$

$$2) \text{ Nanoparticle yield (\%)} = \frac{\text{weight of NPs}}{\text{weight of drug fed initially}} \times 100\%$$

where weight of drug in NPs is calculated from the absorbance of NP dispersions, weight of NPs is taken after lyophilization.

The hydrodynamic diameter and size distribution of the particles dispersed in super-purified water were measured at room temperature with a particle DLS analyzer model Nanophox (Sympatec GmbH, Germany). Dried particle size and size distribution were measured with a Scanning Electron Microscope (SEM). SEM pictures were obtained with a JEOL, JSM-840 Model (Japan). For this purpose, a drop of dilute particle dispersion in super-purified water was spread on a glass surface, and then dried

at room temperature. The dried samples were coated with carbon in vacuum before viewing under a SEM. The average particle size and distribution were determined by the measurement of the diameter of more than 200 particles with image analysis software (Analysis Auto, Soft Imaging System GmbH, Germany).

### Particle Stability

In order to check the stability of the proteinoid particles in a dispersion, ζ-potential was measured by a WALLIS ζ-potential analyzer (Cordouan Technologies, France). The ζ-potential of NPs was analyzed at the pH range of 2.8-10.8 at a concentration of 10 mg/mL.

Proteinoid NP aqueous dispersions (1 mg/mL) were put in a refrigerator at 4 °C for 6 months. The dispersions were checked by Nanophox for their size and size distribution and by HPLC for their drug content. Additionally, in order to check the particle stability after drying, the particles were freeze-dried and then redispersed in an aqueous phase to their original concentration. The samples' size and size distribution were then rechecked by Nanophox.

### PEGylation of the Dox-loaded Proteinoid NPs

PEGylated Dox-loaded proteinoid NPs were prepared by an initial reaction of the primary amine groups on the surface of the proteinoid NPs with NHS-PEG-maleimide. Briefly, NHS-PEG-maleimide (20 mg) was dissolved in PBS (1 mL). 500 µL of the NHS-PEG-maleimide solution was then added to 2 mL of Dox-loaded NPs (10 mg/mL in PBS) and the reaction was stirred for 1 h at room temperature. The obtained PEGylated Dox-loaded NPs, named PEG-Dox-loaded NPs, were then washed from excess reagents by extensive dialysis against super-purified water. Following dialysis, 10% v/v of 1M bicarbonate buffer was added to the PEG-Dox-loaded NPs. Blocking of residual amine groups was then accomplished by adding 50 mg of glycine to the PEG-Dox-loaded NP aqueous dispersion. Hollow proteinoid NPs were also PEGylated by the same procedure. The PEGylated NPs were characterized by DLS for their size and size distribution as described above.

### In vitro Drug Release Study

*In vitro* release of Dox from Dox-loaded NPs and PEG-Dox-loaded NPs was carried out under sink conditions (drug concentration in the medium was kept five times lower than the saturation solubility of Dox in buffer). Particle samples were suspended in PBS to give a final concentration of 0.5 mg/mL. NP suspensions in PBS, human serum and human blood were prepared to a final concentration of 20% NPs v/v. All the samples were placed in a shaker with a constant agitation at 37 °C. Periodically, the samples were filtered through a centrifugation tube (Vivaspin 30 kDa MWCO) and supernatant samples were taken at each time point. The concentration of released Dox in each sample was determined by the absorbance at 487 nm, taking the initial concentration of Dox within the NPs as an absolute value. Dox concentrations were determined using a calibration curve of known Dox concentrations, as described above. The study was performed in sample triplicates.

### Cell Proliferation Analysis by XTT

*In vitro* toxicity of hollow NPs, non-PEGylated and PEGylated Dox-loaded NPs was tested using an XTT (2,3-bis-(2-methoxy-4-nitro-5-sulfophenyl)-2H-tetrazolium-5 carboxanilide salt) assay on A172 human glioblastoma cells, HCT116 human colon

carcinoma and MDA-MB-231 human invasive ductal carcinoma. The cells were treated with hollow NPs and Dox-loaded NPs, both PEGylated and non-PEGylated. Treatment with Dox-containing NPs, PEGylated and non-PEGylated, was done at two concentrations: 0.01 and 0.05 mg/mL with 1.66  $\mu$ g and 8.3  $\mu$ g Dox, respectively. Hollow PEGylated and non-PEGylated NP treatment was done only with the higher concentration of 0.05 mg/mL. Cells treated with an equivalent amount of free Dox and untreated cells served as control groups. Human glioblastoma cells were seeded in a 96 well-plate at a density of  $1 \times 10^5$  cells/well with 100  $\mu$ L culture medium and grown in a humidified 5% CO<sub>2</sub> atmosphere at 37 °C before the addition of the samples. Next, Dox-loaded NP samples dispersed in the culture medium were added to a 96 well-plate, giving a final concentration of 0.01 mg/mL and 0.05 mg/mL of NPs per well. After incubation for 48 h at 37 °C, the 50  $\mu$ L XTT solution was added to each well according to the kit manufacturer instructions. The percentage of cell cytotoxicity was calculated as shown in the manufacturer protocol for the XTT toxicity detection kit [30]. All samples were tested in sixfold.

### Cytokines Induction Assay

The secretion levels of three different inflammatory interleukins were tested using IL-6 and TNF- $\alpha$  as a model for the innate immune response and IL-10 as a model for the late immune response. Cytokines induction assay was performed according to literature [31].

The effect of Dox-loaded NPs, in the presence or absence of bound PEG, on TNF- $\alpha$ , IL-10 and IL-6 cytokines secretion from human Peripheral Blood Mononuclear Cells (PBMCs) was tested. PBMCs were freshly isolated from the blood of 3 healthy human donors obtained from Tel Hashomer (Sheba) blood bank. Whole blood of each human was diluted with PBS/- in a volume ratio of 1:1. Samples containing 4 mL of diluted blood were then gently overlaid onto 3 mL Ficoll (3:4 ratio). A gradient was then obtained by centrifugation at 22 °C, 1400 rpm for 35 min. Opaque-light PBMCs ring was removed from the interphase into a new tube. PBMCs were washed with PBS/- and then centrifuged at 1400 rpm for 10 min. Each PBMC pellet was resuspended in a PBMC growth medium (with 5% fetal bovine serum and 1% penicillin/streptomycin solution) to which PBS dispersions of either the Dox-loaded NPs or PEG-Dox-loaded NPs were added. The final concentration of each 1 mL well (24 well-plates) contained  $3 \times 10^6$  cells and 0.05 mg NPs. LPS was used as a positive control (100 ng/mL) and PBS/- as a negative control. The different 24 well-plates were then incubated at 37 °C humidified, 5% CO<sub>2</sub> for 2 and 24 h. Upon incubation, at each time interval, the cells were centrifuged at 1400 rpm for 10 min and the supernatant was removed and stored in -80 °C freezer for further quantification of secreted cytokines. Human cytokines TNF- $\alpha$ , IL-10 and IL-6 levels were determined using human IL-6 E, IL-10 and TNF- $\alpha$  ELISA kits according to the manufacturer instructions.

## Results and Discussion

### Preparation of Proteinoids by Thermal Condensation Polymerization

All the polymers were produced via a simple thermal condensation reaction which utilizes the carboxylate and amine groups of an amino acid side chain or those at the  $\alpha$ -position [32]. To obtain a product with good yield by a thermal condensation reaction, anhydrous conditions and inert atmosphere are required [33]. Lysine plays the main role in this process. It promotes the initiation of the

polymerization and determines the basic nature of the resulting proteinoids [34]. Histidine was chosen for its imidazole group which can facilitate a proton influx, known as the proton sponge effect, to endosomes, leading to endosomal/lysosomal escape [35]. Also, it is well known that the interaction of a guanidinium-head group of arginine with membrane phospholipids enhances membrane permeability [36]. The combination of histidine and arginine motives in the proteinoids can both promote endosomal escape and increase the efficiency of internalization through the endocytic pathway [37,38].

Four different basic-nature proteinoids were obtained using thermal condensation polymerization. To evaluate the different nature of various proteinoid compositions, the percentages of histidine and phenylalanine were varied from 35% and 15% in P(KRHF-PLLA) 35:15 to 20% and 30% in P(KRHF-PLLA) 20:30, respectively, whereas the composition of lysine, arginine, and PLLA was kept constant, as presented in Table 1.

Table 2 depicts the molecular weights, polydispersity indices (PDI), and optical activity measurements of the obtained proteinoids. The thermal condensation polymerization that yields proteinoids is a random process and as such is known to yield low molecular weight polymers with high polydispersity [39,40]. The presented method surprisingly allows to synthesize polymers with a very low PDI and relatively high molecular weights using thermal polycondensation by maintaining certain reaction conditions [23, 24]. As can be seen in the table, all polymers have high molecular weights, ranging from 122 to 149 kDa. Also, as mentioned previously, the PDIs of the polymers are very low, at the range of 1.01-1.03. It should be noted that the 2 kDa PLLA is fully polymerized within the proteinoid backbone, as no corresponding peak was observed. Although they undergo a high temperature procedure which causes transitions, overall, the proteinoids remain optically active. This may become useful in many biological applications [23].

**Table 2:** Mw, Mn, Mp, polydispersity and optical activity of the various proteinoids.

Proteinoid <sup>a</sup>	Mw (Da) <sup>b</sup>	Mn (Da) <sup>b</sup>	Mp (Da) <sup>b</sup>	PDI <sup>c</sup>	Optical Activity [ $\alpha$ ] <sub>D</sub> <sup>25 °C</sup> (°) <sup>d</sup>
P(KRHF-PLLA) 35:15	133400	129600	129200	1.03	- 4.2
P(KRHF-PLLA) 30:20	122400	121400	123800	1.01	-34.2
P(KRHF-PLLA) 25:25	140800	139400	136900	1.01	-27.8
P(KRHF-PLLA) 20:30	149300	146000	142400	1.02	-65.6

<sup>a</sup>The proteinoids were prepared according to the experimental section; <sup>b</sup>molecular masses were measured by GPC, Mp is the molecular mass at the peak; <sup>c</sup>PDI is the polydispersity index, given by Mw/Mn; <sup>d</sup>specific optical rotation ( $c=1$ , in H<sub>2</sub>O, at 25 °C).

Table 3 presents the thermal properties of the proteinoids investigated by DSC and TGA, as described above. The melting temperatures of the different proteinoids varied at 295-337 °C. As can be noticed, the range of temperatures is not wide, and the reason lies in their monomeric composition. While decreasing the ratio of histidine to phenylalanine from 35:15 to 20:30, the melting point of the proteinoids increased from 295 °C to 337 °C, probably since the increasing relative amount of phenylalanine enhances the rigidity and the mechanical properties of the proteinoid.

TGA measurements of the proteinoids depict a similar pattern in the decomposition temperatures. These temperatures vary from 339 °C up to 426 °C. The weight loss at 400 °C of all proteinoids was in the range of 46-52%. P (KRHF-PLLA) 20:30, with 30% phenylalanine, has the highest decomposition temperature of 426 °C, and it lost 46% of the initial weight at 400 °C. This can be explained by its increased rigidity, caused by the increased relative amount of phenylalanine.

**Table 3:** Thermal properties of proteinoids produced by thermal polymerization.

Proteinoid	T <sub>m</sub> (°C) <sup>a</sup>	ΔH <sub>m</sub> (J/g) <sup>a</sup>	Weight loss (%) <sup>b</sup>	T <sub>dec</sub> (°C) <sup>c</sup>
P(KRHF-PLLA) 35:15	295	-270	52	339
P(KRHF-PLLA) 30:20	302	-447	48	355
P(KRHF-PLLA) 25:25	308	-513	47	362
P(KRHF-PLLA) 20:30	337	-567	46	426

<sup>a</sup>T<sub>m</sub> and ΔH<sub>m</sub> were measured by DSC; <sup>b</sup>weight loss was measured by TGA at 400 °C; <sup>c</sup>T<sub>dec</sub> (temperature of decomposition) was measured by TGA/DSC and refers to the exothermal peak in DSC.

#### Preparation of Hollow and Dox-loaded Proteinoid Nanoparticles

As described above, the hollow and Dox-loaded proteinoid NPs were formed by a self-assembly mechanism. All proteinoids self-assembled to obtain hollow proteinoid NPs, as well as 15% Dox-loaded NPs, by the procedure described above. In order to select the best candidate for further research, size and ζ-potential measurements were performed. Table 4 summarizes the sizes and ζ-potentials of the hollow and Dox-loaded proteinoid NPs. As can be seen in the table, the smallest hollow and Dox-loaded particles were synthesized using P(KRHF-PLLA) 20:30. The Dox-loaded particles formed from the same proteinoid also had the highest ζ-potential, 16.6 Mv, which makes them the most stable due to their low tendency to aggregate in aqueous media.

**Table 4:** Characteristics of hollow and 15% Dox-loaded proteinoid NPs.

Proteinoid	Size of hollow NPs (nm) <sup>a</sup>	Size of Dox-loaded NPs (nm) <sup>a</sup>	ζ-potential (mV) of Dox-loaded NPs <sup>b</sup>
P(KRHF-PLLA) 35:15	256.7 ± 41.9	100.3 ± 38.7	8.8
P(KRHF-PLLA) 30:20	32.1 ± 5.7	302.2 ± 31.8	8.1
P(KRHF-PLLA) 25:25	278.5 ± 30.5	193.4 ± 31.6	10.1
P(KRHF-PLLA) 20:30	36.2 ± 6.9	111.5 ± 15.2	16.6

<sup>a</sup>Particle size and size distribution of hollow NPs and the Dox-loaded NPs were measured by DLS; <sup>b</sup>ζ-potential of Dox-loaded NPs was measured by a ζ-potential analyzer at a concentration of 10 mg/mL and pH of 7.4.

In order to optimize the loaded Dox concentration, P(KRHF-PLLA) 20:30 Dox-loaded NPs with varied initial Dox concentration were analyzed to estimate their size and the Dox entrapment efficiency within the NPs. Table 5 shows that generally, as the Dox concentration increases, the size of the NPs increases.

The optimal entrapment efficiency of 93 ± 12% was achieved by using an initial Dox concentration of 15%. The size of hollow P (KRHF-PLLA) 20:30 NPs was 36.2 ± 6.9 nm, while the size of the Dox-loaded NPs was 111.5 ± 15.2 nm. Based on the presented

data, 15% Dox-loaded P(KRHF-PLLA) 20:30 NPs were chosen as the optimal NPs for further research. This result competes with the Dox concentration in the commercial drug Doxil, in which 12.5% was an optimum [12]. Rising above this concentration, higher entrapment efficiency was not achieved.

**Table 5:** Characteristics of Dox-loaded P(KRHF-PLLA) 20:30 NPs.

Drug fed initially (%) <sup>a</sup>	NP formation yield (%) <sup>b</sup>	Entrapment efficiency (%) <sup>b</sup>	Size of NPs (nm) <sup>c</sup>
10	99	73 ± 11	96.5 ± 16.1
15	97	93 ± 12	111.5 ± 15.2
25	94	87 ± 11	116.7 ± 2.0
30	98	85 ± 14	880.8 ± 475.4

<sup>a</sup>Initial drug concentration that was put in the self-assembly reaction vessel; <sup>b</sup>percentages of NP formation and entrapment are calculated as described in section 2.4; <sup>c</sup>particle size and size distribution of hollow NPs and the Dox-loaded NPs were measured by DLS.

#### Characterization of Proteinoids and Dox-loaded NPs

The FTIR spectra of the free Dox, proteinoid P(KRHF-PLLA) 20:30 and Dox-loaded NPs are shown in Figure 3. The IR spectrum of free Dox is represented in (A). In this spectrum, a pair of doublets at 3415/3331 cm<sup>-1</sup> and at 3023/2926 cm<sup>-1</sup> is clearly shown. The first doublet (at 3415/3331 cm<sup>-1</sup>) can be associated with the H-bonded O–H stretch and N–H stretch (amide I). The second doublet (at 3023/2926 cm<sup>-1</sup>) corresponds to the C–H stretching of methyl groups and aromatic rings. The peaks at 802 cm<sup>-1</sup> and 776 cm<sup>-1</sup> are due to the primary amine NH<sub>2</sub> wag and N–H deformation bonds, respectively [41]. The IR spectrum of the proteinoid shown in (B) clearly shows the presence of the groups derived from the amino acids and PLLA, with characteristic peaks at 2934 cm<sup>-1</sup> (corresponding to the C–H alkyl stretching band), at 1664 cm<sup>-1</sup> (corresponding to the carbonyl C=O vibration, and N–H bend - amide I), at 1537 cm<sup>-1</sup> (amide II) and at 1117 cm<sup>-1</sup> (corresponding to the stretching of C–O bonds of ester groups). The IR spectrum of the Dox-loaded NPs in (C) shows the proteinoid characteristic peaks, with a small left-shift. In addition, the IR spectrum of Dox-loaded NPs shows a broad peak at 3369 cm<sup>-1</sup>, a small peak at 2942 cm<sup>-1</sup>, which can be associated with amide I and C–H stretching coming from Dox, and a broad peak at 802 cm<sup>-1</sup>. The broadening and shifting of existing peaks in the proteinoid NPs can be associated with the encapsulation of Dox and self-assembly reorganization of proteinoid chains due to NP formation.

XRD analysis of free Dox along with the proteinoid and freeze-dried Dox-loaded NPs is also shown in Figure 3. Free Dox (D) shows clear peaks in the diffractogram indicating the presence of a crystalline phase in its native form, whereas the proteinoid in (E) shows a typical amorphous pattern, as expected for a random polymerization product. The reduction in number and intensity of the peaks and absence of several peaks in the XRD pattern of Dox-loaded NPs in comparison to the free drug, also indicates the phase transformation of crystalline doxorubicin to amorphous doxorubicin [42].

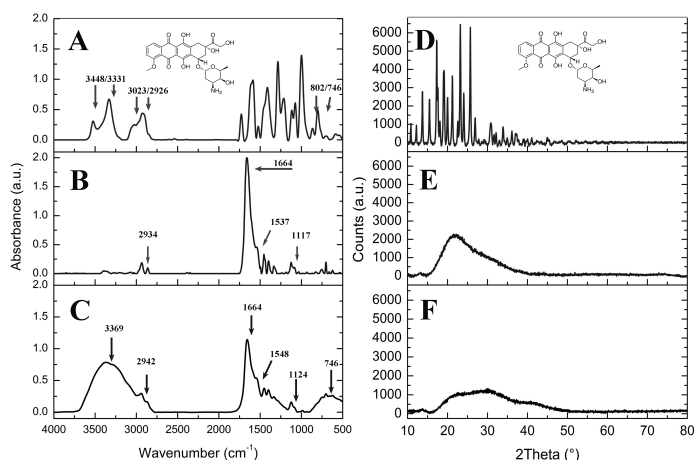


**Figure 3:** FTIR spectra and XRD diffraction patterns of free Dox (A and D), proteinoid P(KRHF-PLLA) 20:30 (B and E), and P(KRHF-PLLA) 20:30 15% Dox-loaded NPs (C and F), respectively.

To verify the encapsulation of Dox within the NPs, characterization of doxorubicin in a solution was performed [43]. The absorbance spectra of free Dox and Dox-loaded NPs containing the same amount of Dox, were measured in physiological pH (7.4) and after proteinoid dissolution at pH 2, as shown in Figure 4. The main absorption peak of Dox occurred at 487 nm at both tested pHs. The main absorption peak at pH 2 was shaped similarly to Dox, however, at pH 7.4 the intensity of the main absorption peak of the Dox-loaded NPs was much lower than the intensity of the main peak of free Dox. This indicates the encapsulation of the drug within the NPs. Additionally, it is seen that at pH 2 the absorption peaks of the Dox-loaded NPs and the free Dox are similar. This fact reveals the release of loaded Dox from the disrupted NPs at this pH.

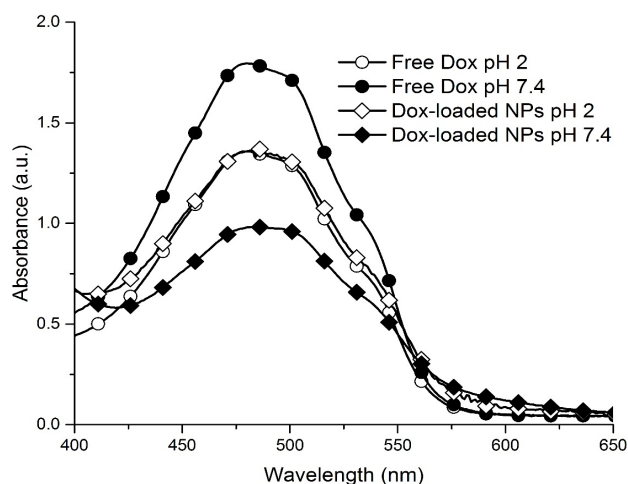


**Figure 4:** Absorbance of free Dox and Dox-loaded NPs at pH 7.4 and pH 2.

Figure 5 shows a typical SEM image (A) of the dry Dox-loaded NPs. The measured diameter is  $51.7 \pm 3.1$  nm, whereas the hydrodynamic diameter shown in the DLS histogram (B) of the Dox-loaded NPs is  $117 \pm 31$  nm. The difference in diameters is

explained by the very hydrophilic character of the proteinoid NPs, causing adsorption of many water molecules on their surface, which are taken into account in the measurement [24].

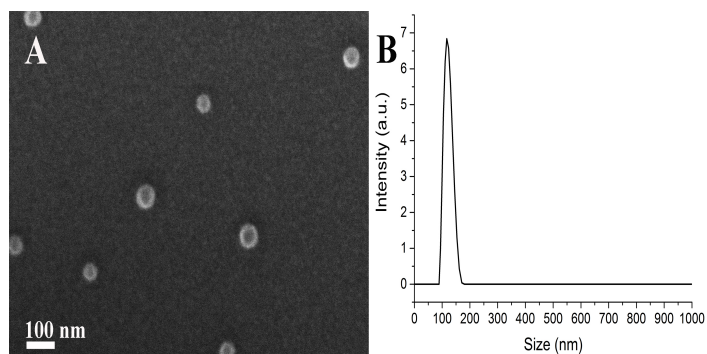


**Figure 5:** A typical SEM image (A) and DLS histogram (B) of 15% Dox-loaded P(KRHF-PLLA) 20:30 NPs.

### Particle Stability

The stability of the hollow, and Dox-loaded P(KRHF-PLLA) 20:30 NPs was studied using  $\zeta$ -potential measurements, shown in Figure 6. The hollow P(KRHF-PLLA) 20:30 NPs were positively charged at acidic (2.83) and neutral (7.4) pH, 2.7 mV and 3.5 mV, respectively, whereas at pH 10.88 the NPs demonstrated a negative charge with -9.0 mV due to the carboxylate groups attached to the surface of the particles. The isoelectric point of the hollow P(KRHF-PLLA) 20:30 NPs was at pH 7.7. The  $\zeta$ -potential of Dox-loaded P(KRHF-PLLA) 20:30 NPs was positive at pH values ranging between acidic and neutral, similarly to the hollow P(KRHF-PLLA) 20:30 NPs. However, with pH in the range of 5.5 to 7.4, the  $\zeta$ -potential increased from 5.65 mV at pH 5.5 up to 16.6 mV at pH 7.4. This increase in the  $\zeta$ -potential can be explained by the protonation of the amine group ( $pK_a$  7.6) of the loaded Dox within the NPs [44]. The isoelectric point of the Dox-loaded P(KRHF-PLLA) 20:30 NPs shifted to pH 8.9, and when the pH increased to 10.48, the  $\zeta$ -potential decreased to -3.29 mV. The decrease in  $\zeta$ -potential in Dox-loaded NPs is less drastic compared to the hollow P(KRHF-PLLA) 20:30 NPs, probably due to the different self-assembly conditions used for the Dox encapsulation.

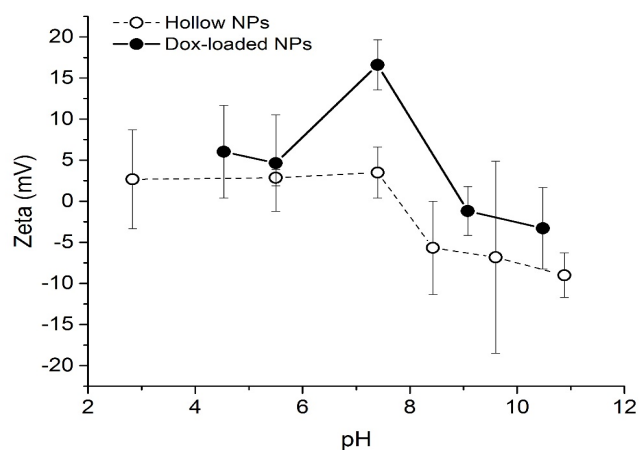


**Figure 6:**  $\zeta$ -potential of the hollow and Dox-loaded P(KRHF-PLLA) 20:30 NPs as function of pH. Each point on the graph is an average of ten performed measurements. To ensure PEG conjugation to the Dox-loaded P(KRHF-PLLA)

20:30 NPs,  $\zeta$ -potential of the PEGylated NPs was studied using the same procedure. Figure 7 illustrates that  $\zeta$ -potential of PEG-Dox-loaded NPs varied around zero in the pH range of 2.8 to 10.15. As shown earlier, the  $\zeta$ -potential of the Dox-loaded NPs has changed with the pH increase. The decreasing of  $\zeta$ -potential of the PEG-Dox-loaded NPs to zero (especially in pH 7.4) can be explained by the PEG conjugation to the free amino groups of the Dox-loaded NPs and confirms the successful PEGylation.

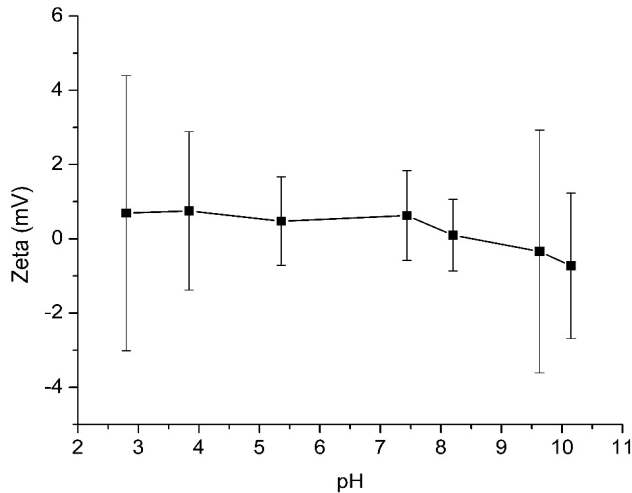


**Figure 7:**  $\zeta$ -potential of the PEG-Dox-loaded P(KRHF-PLLA) 20:30 NPs as function of pH. Each point on the graph is an average of ten performed measurements.

NP stability was also determined at different storage conditions: in dispersion at refrigerating conditions over time and after freeze-drying. Proteinoid NP aqueous dispersions (1 mg/mL) kept in a refrigerator at 4 °C for 6 months remained the same size and size distribution, while keeping the drug content constant. Additionally, in order to check particle stability after drying, the particles were freeze-dried and then redispersed in an aqueous phase to their original concentration. The samples' size and size distributions were not affected by this procedure. This provides two types of storing conditions for further applications with the NPs.

#### In vitro Drug Release Study

The *in vitro* release study of Dox from P(KRHF-PLLA) 20:30 NPs was carried out after NP PEGylation, as described, in various media: PBS, human serum and human whole blood. It should be noted that the NPs size after PEGylation is  $154 \pm 15$  nm. Figure 8 shows the *in vitro* release profile of Dox from Dox-loaded and from PEGylated Dox-loaded P(KRHF-PLLA) 20:30 NPs.

A variety of factors affect the rate of drug release, such as the polymeric structure, the drug itself, the pH of the medium, etc. The effects of PEGylation of the NPs and the effect of the environment on the release rate of Dox from the NPs were investigated. The release of Dox from non-PEGylated Dox-loaded P(KRHF-PLLA) 20:30 NPs when dispersed in serum and blood was very rapid. However, the rate of Dox release in a PBS dispersion was notably lower. The maximum release of Dox from the NPs was 99% within 24 h, in blood and serum. In PBS, over 24 h, the drug release was only about 40%. The PEGylated NPs have shown a different drug release pattern. The percent of Dox which was released from the

PEGylated NPs in human blood reached 87% within 5 h. Contrarily, in PBS and human serum the release of the drug from the NPs was very slow, with a maximum release of 7% over 24 h. This fact can be explained by the assumption that PEGylation of the NPs yields better packaging, with less degradable bonds on the surface of the NPs, which cause the rate of the drug release to be decreased [45]. The high release in blood is attributed to the enzymes which degrade the proteinoid backbone, through hydrolysis of the esters of the PLLA and the peptide bonds [39,46].

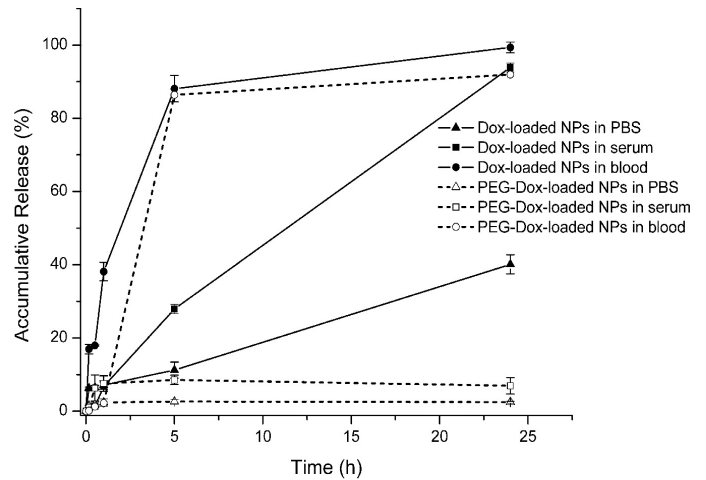


**Figure 8:** Release of Dox from non-PEGylated and PEGylated Dox-loaded P(KRHF-PLLA) 20:30 NPs in PBS, human serum and human blood over time. Each point represents mean  $\pm$  standard deviation of 3 separate samples.

#### Cell Proliferation Assay by XTT

*In vitro* effect of the non-PEGylated and PEGylated Dox-loaded P(KRHF-PLLA) 20:30 NPs on cell proliferation of human A172 glioblastoma, MDA-MB-231 ductal carcinoma and HCT116 colon carcinoma cells was tested using XTT, as described in the experimental part. Figure 9 illustrates the results of the performed XTT experiments of A172 (A), MDA-MB231 (B) and HCT116 (C) cells. Hollow NPs and PEGylated hollow NPs, which served as a control, do not possess any toxicity, showing cell viability levels of 108-119% and 100-103%, respectively, after treatment with a high dose of 0.05 mg/mL. This means that the proteinoid NPs themselves are non-toxic to the body, as expected. However, Dox-loaded NPs, either non-PEGylated or PEGylated, showed low cell viability levels of close to 40%, after treatment with a low dose of 0.01 mg/mL (Dox concentration  $1.66 \mu\text{g/mL}$ ). Furthermore, this cytotoxic effect is similar to the effect achieved with free Dox at the same concentration. When the concentration of the treating NPs was raised to 0.05 mg/mL ( $8.3 \mu\text{g/mL}$ ) both kinds of NPs were found more toxic, while PEGylated NPs achieved even greater toxicity than that of the free Dox.

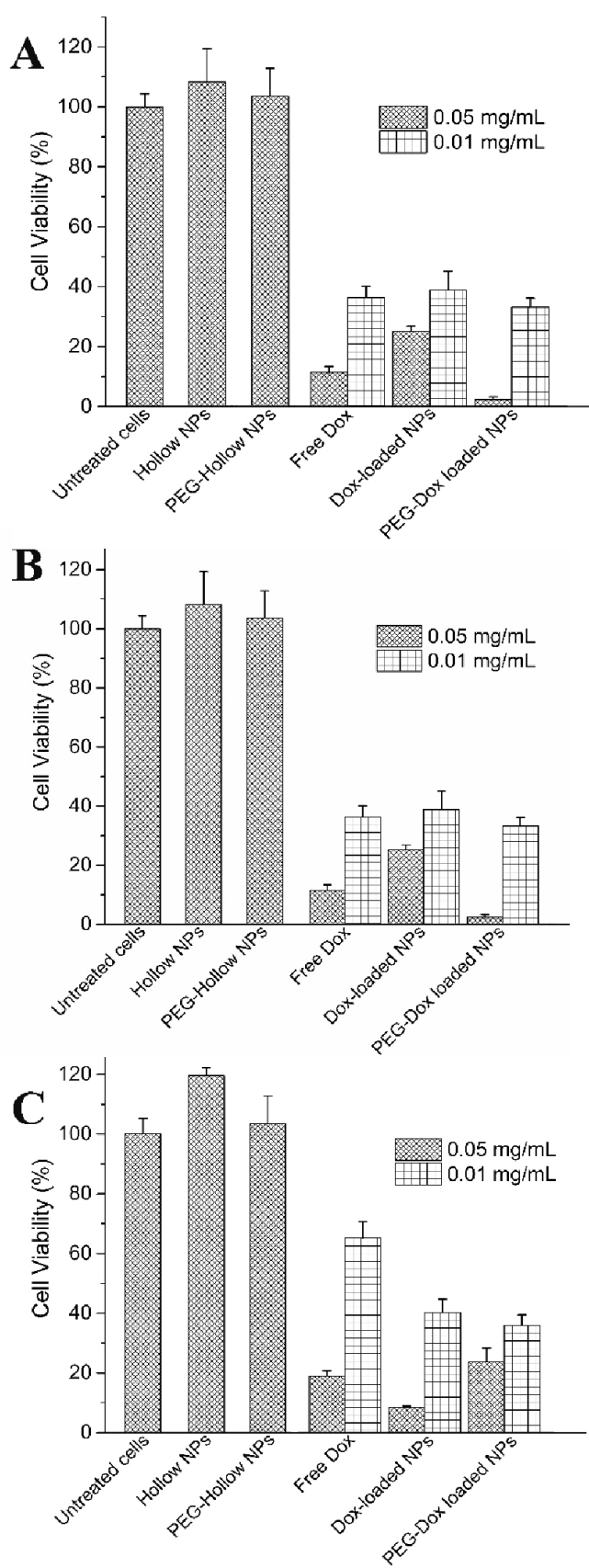


**Figure 9:** Cell viability of human A172 glioblastoma (A), MDA-MB-231 ductal carcinoma (B) and HCT116 colon carcinoma (C)

cells 48 h post-treatment measured by XTT assay. Cells were treated with 0.01 and 0.05 mg/mL NPs and an equivalent amount free of Dox. Hollow NPs, PEG NPs and untreated cells served as control. Each bar represents mean  $\pm$  standard deviations of six separate samples.

### Cytokines Induction Assay

In order to evaluate the safety profile of the P(KRHF-PLLA) 20:30 NPs as a future drug delivery vehicle, an *ex vivo* cytokine induction study was performed using human Peripheral Blood Mononuclear Cells (PBMCs), to examine the secretion of major inflammatory cytokines. The results are summarized in Table 6. Neither the non-PEGylated Dox-loaded NPs nor the PEGylated ones caused an elevated secretion of both innate and late cytokine response at 2 h and 24 h of treatment with the particles. As a positive control, we used the TLR4 natural ligand and LPS that secreted high levels of both TNF- $\alpha$  and IL-6 after only 2 h of incubation with an increase after 24 h of exposure to the LPS. IL-10 was secreted after 24 h, as expected.

**Table 6:** Effect of Dox-loaded NPs, in presence or absence of bound PEG, on the secretion of TNF- $\alpha$ , IL-10 and IL-6 in human PBMCs 2 h and 24 h of incubation.

Treatment	TNF- $\alpha$ (pg/mL) <sup>a</sup>		IL-6 (pg/mL) <sup>a</sup>		IL-10 (pg/mL) <sup>a</sup>	
	2 h	24 h	2 h	24 h	2 h	24 h
Negative control (PBS)	N.D.	N.D.	N.D.	N.D.	N.D.	N.D.
Positive control (LPS)	6586 $\pm$ 1591	16697 $\pm$ 8875	1788 $\pm$ 782 <sup>b</sup>	2480 $\pm$ 321 <sup>b</sup>	N.D.	669 $\pm$ 42 <sup>b</sup>
Dox-loaded NPs	N.D.	N.D.	N.D.	N.D.	N.D.	N.D.
PEG-Dox-loaded NPs	N.D.	N.D.	N.D.	N.D.	N.D.	N.D.

<sup>a</sup>Values are expressed as means  $\pm$  standard deviation, N.D. – not detectable; <sup>b</sup>upper limit of quantification.

### Conclusions

In this study, lysine-based proteinoids were produced via a simple thermal condensation reaction. The proteinoids composed of L-lysine, L-arginine, L-histidine, L-phenylalanine and PLLA, achieved high molecular weights with narrow size distributions and possess optical activity; thus, they may be utilized for drug delivery. The thermal stability of the proteinoids was tested and it increased with the relative ratio of phenylalanine, which was chosen for its rigidity. Hollow and drug-loaded NPs with narrow size distribution were produced using a self-assembly method. NPs with various drug concentrations were synthesized, and the NPs with optimal size,  $\zeta$ -potential and entrapment efficiency were chosen for further study. It was demonstrated that it is possible to conjugate PEG to the drug-loaded NPs in order to enhance the NP stability and prevent leakage of the drug. The findings confirmed that the PEGylated Dox-loaded NPs are more stable in all environments and the release of the drug occurs only in the blood, as intended.

In future study, the PEGylated Dox-loaded NPs will be tested *in vivo* using a mouse model to explore the body distribution and half lifetime in the blood. Moreover, conjugation of suitable

targeting agents to the PEGylated Dox-loaded NPs will probably enhance the specific delivery to tumors and increase their affinity. Our intention is to achieve better specificity and targeting to treat cancer better than the currently available Doxil. Additionally, the proteinoid NPs may be used to encapsulate other anti-cancer drugs, such as taxol, and even combine drug delivery and tumor tagging by encapsulation of a drug and a dye in one NP.

### Acknowledgements

This study was supported by the Israeli Ministry of Commerce and Industry (Kamin Grant). The authors thank Dr. Safra Rudnick-Glick for her assistant with the immunogenic studies.

### References

1. Reddy LH, Murthy RS (2004) Pharmacokinetics and biodistribution studies of Doxorubicin loaded poly(butyl cyanoacrylate) nanoparticles synthesized by two different techniques. *Biomed Pap* 148: 161-166.
2. Rafiyath SM, Rasul M, Lee B, Wei G, Lamba G, et al. (2012) Comparison of safety and toxicity of liposomal doxorubicin vs. conventional anthracyclines: a meta-analysis. *Exp Hematol Oncol* 1: 1-10.
3. Talelli M, Iman M, Varkouhi AK, Rijcken CJF, Schiffelers RM, et al. Core-crosslinked polymeric micelles with controlled release of covalently entrapped doxorubicin. *Biomaterials* 31: 7797-7804.
4. Hershman DL, McBride RB, Eisenberger A, Tsai WY, Grann VR, et al. (2008) Doxorubicin, cardiac risk factors, and cardiac toxicity in elderly patients with diffuse B-cell non-Hodgkin's lymphoma. *J Clin Oncol* 26: 3159-3165.
5. Chatterjee K, Zhang J, Honbo N, Karliner JS (2010) Doxorubicin cardiomyopathy. *Cardiology* 115: 155-162.
6. Canal F, Sanchis J, Vicent MJ (2011) Polymer-drug conjugates as nano-sized medicines. *Curr Opin Biotechnol* 22: 894-900.
7. Mauro N, Campora S, Adamo G, Scialabba C, Ghersi G, et al. (2016) Polyaminoacid-doxorubicin prodrug micelles as highly selective therapeutics for targeted cancer therapy. *RSC Adv* 6: 77256-77266.
8. Shi M, Lu J, Shoichet MS (2009) Organic nanoscale drug carriers coupled with ligands for targeted drug delivery in cancer. *J Mater Chem* 19: 5485-5498.
9. Aggarwal P, Hall JB, McLeland CB, Dobrovolskaia MA, McNeil SE (2009) Nanoparticle interaction with plasma proteins as it relates to particle biodistribution, biocompatibility and therapeutic efficacy. *Adv Drug Deliv Rev* 61: 428-437.
10. Varanda LC, Júnior MJ, Beckjúnior W (2011) Magnetic and multifunctional magnetic nanoparticles in nanomedicine: challenges and trends in synthesis and surface engineering for diagnostic and therapy applications. in: A. Laskowsky (Ed.), *Biomed Eng Trends Mater Sci InTech* 397-424.
11. Soundararajan A, Squamous N, Carcinoma C, Model X (2010) [(186)Re]Liposomal doxorubicin (Doxil): in vitro stability, pharmacokinetics, imaging and biodistribution in a head and neck squamous cell carcinoma xenograft model. *Surgery* 36: 515-524.
12. (Chezy) Barenholz Y (2012) Doxil® — The first FDA-approved nano-drug: lessons learned. *J Control Release* 160: 117-134.
13. Zhang L, Chan JM, Gu FX, Rhee J, Wang AZ, et al. (2008) Self-assembled lipid polymer hybrid nanoparticles: a robust drug delivery platform, *ACS Nano*. 2: 1696-1702.
14. Gabizon A, Shmeeda H, Barenholz Y (2003) Pharmacokinetics of pegylated liposomal Doxorubicin: review of animal and human studies, *Clin.Pharmacokinet.* 42: 419-436.
15. Fox SW (1960) How did life begin?. *Science* 132: 200-208.
16. Fox SW (1995) Thermal synthesis of amino acids and the origin of life. *Geochim Cosmochim Acta* 59: 1213-1214.
17. Fox SW, Jungck JR, Nakashima T (1974) From proteinoid microsphere to contemporary cell: formation of internucleotide and peptide bonds by proteinoid particles. *Orig Life* 5: 227-237.
18. Fox S, Harada K (1960) The thermal copolymerization of amino acids common to protein. *J Am Chem Soc* 82: 3745-3751.
19. Fox SW, Harada K (1962) Thermal polymerization of amino acid mixtures containing aspartic acid or a thermal precursor of aspartic acid, U.S. Patent No. 3,052,655.
20. Dose K (1974) Chemical and catalytical properties of thermal polymers of amino acids (proteinoids). *Orig Life* 5: 239-252.
21. Rohlfling DL, Fox SW (1969) Catalytic activities of thermal polyanhydro- $\alpha$ -amino acids. in: *Adv Catal Related Subj*, Daniel Dou, Elsevier Ltd 20: 373-418.
22. Cohen-Arazi N, Hagag I, Kolitz M, Domb AJ, Katzhendler J (2010) Biodegradable polymers derived from amino acids for biological applications. *Adv Sci Technol* 76: 30-35.
23. Kolitz-Domb M, Margel S (2014) Engineered narrow size distribution high molecular weight proteinoids, proteinoid-poly(L-lactic acid) copolymers and nano/micro-hollow particles for biomedical applications. *J Nanomed Nanotechnol* 5: 1-10.
24. Kolitz-Domb M, Corem-Salkmon E, Grinberg I, Margel S (2014) Synthesis and characterization of bioactive conjugated near-infrared fluorescent proteinoid-poly(L-lactic acid) hollow nanoparticles for optical detection of colon cancer. *Int J Nanomedicine* 9: 5041-5053.
25. Quirk S (2009) Triggered release of small molecules from proteinoid microspheres. *J Biomed Mater Res - Part A* 91: 391-399.
26. Quirk S (2013) Enhanced catalytic activity from proteinoid microspheres. *J Biomed Mater Res - Part A* 101: 1133-1143.
27. Ma X, Santiago N, Chen YS, Chaudhary K, Milstein SJ, et al (1994) Stability study of drug-loaded proteinoid microsphere formulations during freeze-drying. *J Drug Target* 2: 9-21.
28. Kolitz-Domb M, Grinberg I, Corem-Salkmon E, Margel S (2014) Engineering of near infrared fluorescent proteinoid-poly(L-lactic acid) particles for in vivo colon cancer detection. *J Nanobiotechnology* 12: 30-43.
29. Kolitz-Domb M, Margel S (2015) Engineering of novel proteinoids and PLLA-proteinoid polymers of narrow size distribution and uniform nano/micro-hollow particles for biomedical applications. in: P Sera, Andrea (Ed.), *Adv Bioeng* 51-77.
30. Industries B (2012) Cell proliferation kit XTT based.
31. Landesman-Milo D, Goldsmith M, Leviatan Ben-Arye S, Witenberg B, Brown E, et al. (2013) Hyaluronan grafted lipid-based nanoparticles as RNAi carriers for cancer cells. *Cancer Lett* 334: 221-227.
32. Tallawi M (2011) Proteinoid/hydroxyapatite hybrid microsphere composites. *J Biomed Mater Res B Appl Biomater* 96: 261-266.
33. Madhan Kumar AB, Jayakumar R, Rao KP (1996) Synthesis and aggregational behavior of acidic proteinoid. *J Polym Sci*

34. Fox SW, Waehnelde TV (1968) The thermal synthesis of neutral and basic proteinoids, *Biochim Biophys Acta - Protein Structure* 160: 246-249.
35. Jiang T, Zhang Z, Zhang Y, Lv H, Zhou J, et al. (2012) Dual-functional liposomes based on pH-responsive cell-penetrating peptide and hyaluronic acid for tumor-targeted anticancer drug delivery. *Biomaterials* 33: 9246-9258.
36. Liu BR, Huang Y, Winiarz JG, Chiang HJ, Lee HJ (2011) Intracellular delivery of quantum dots mediated by a histidine- and arginine-rich HR9 cell-penetrating peptide through the direct membrane translocation mechanism *Biomaterials* 32: 3520-3537.
37. El-Sayed A, Futaki S, Harashima H (2009) Delivery of macromolecules using arginine-rich cell-penetrating peptides: ways to overcome endosomal entrapment. *AAPS J* 11: 13-22.
38. Futaki S (2005) Membrane-permeable arginine-rich peptides and the translocation mechanisms. *Adv Drug Deliv Rev* 57: 547-558.
39. Xiao L, Wang B, Yang G, Gauthier M (2012) Poly(lactic acid)-based biomaterials: synthesis, modification and applications. in: N Ghista, Dhanjo (Ed.), *Biomed Sci Eng Technol, InTech* 249-283.
40. Stille JK (1981) Step-growth polymerization. *J Chem Educ* 58: 862-866.
41. Wu S, Zhao X, Li Y, Du Q, Sun J, et al. (2013) Adsorption properties of doxorubicin hydrochloride onto graphene oxide: Equilibrium, kinetic and thermodynamic studies, *Materials* 6: 2026-2042.
42. Kalaria DR, Sharma G, Beniwal V, V Ravi Kumar MN (2009) Design of biodegradable nanoparticles for oral delivery of doxorubicin: In vivo pharmacokinetics and toxicity studies in rats. *Pharm Res* 26: 492-501.
43. Arora HC, Jensen MP, Yuan Y, Wu A, Vogt S, et al. (2012) Nanocarriers enhance doxorubicin uptake in drug-resistant ovarian cancer cells. *Cancer Res* 72: 769-778.
44. Raghunand N, He X, van Sluis R, Mahoney B, Baggett B, et al. (1999) Enhancement of chemotherapy by manipulation of tumour pH. *Br J Cancer* 80: 1005-1011.
45. Goudoulas TB (2012) Polymers and biopolymers as drug delivery systems in nanomedicine. *Recent Patents Nanomed* 2: 52-61.
46. Gow AJ, Duran D, Malcolm S, Ischiropoulos H, Gow J (1996) Effects of peroxynitrite-induced phosphorylation protein modifications and degradation on tyrosine. *FEBS Lett* 385: 63-66.

**Copyright:** ©2017 Shlomo Margel, et al. This is an open-access article distributed under the terms of the Creative Commons Attribution License, which permits unrestricted use, distribution, and reproduction in any medium, provided the original author and source are credited.